| REPORT DOCUMENTATION PAGE | *Form Approved OMB No. 0704-0188* |
|---|---|



| 1. REPORT DATE *(DD-MM-YYYY)* | 2. REPORT TYPE | 3. DATES COVERED *(From - To)* |
|---|---|---|
| 11-03-2014 | Journal Article | |

**4. TITLE AND SUBTITLE**
Estimation of the barrier layer thickness in the Indian Ocean using Aquarius Salinity

**5a. CONTRACT NUMBER**

**5b. GRANT NUMBER**

**5c. PROGRAM ELEMENT NUMBER**
0602435N

**6. AUTHOR(S)**
Clifford S. Felton, Bulusu Subrahmanyam, V. S. N. Murty, and Jay F. Shriver

**5d. PROJECT NUMBER**

**5e. TASK NUMBER**

**5f. WORK UNIT NUMBER**
73-8677-03-5

**7. PERFORMING ORGANIZATION NAME(S) AND ADDRESS(ES)**
Naval Research Laboratory
Oceanography Division
Stennis Space Center, MS 39529-5004

**8. PERFORMING ORGANIZATION REPORT NUMBER**
NRL/JA/7320--14-2210

**9. SPONSORING/MONITORING AGENCY NAME(S) AND ADDRESS(ES)**
Office of Naval Research
One Liberty Center
875 North Randolph Street, Suite 1425
Arlington, VA 22203-1995

**10. SPONSOR/MONITOR'S ACRONYM(S)**
ONR

**11. SPONSOR/MONITOR'S REPORT NUMBER(S)**

**12. DISTRIBUTION/AVAILABILITY STATEMENT**
Approved for public release, distribution is unlimited.

**13. SUPPLEMENTARY NOTES**

**14. ABSTRACT**
Monthly barrier layer thickness (BLT) estimates are derived from satellite measurements using a multilinear regression model (MRM) within the Indian Ocean. Sea surface salinity (SSS) from the recently launched Soil Moisture and Ocean Salinity (SMOS) and Aquarius SAC-D salinity missions are utilized to estimate the BLT. The MRM relates BLT to sea surface salinity (SSS), sea surface temperature (SST), and sea surface height anomalies (SSHA). Three regions where the BLT variability is most rigorous are selected to evaluate the performance of the MRM for 2012; the Southeast Arabian Sea (SEAS), Bay of Bengal (BoB), and Eastern Equatorial Indian Ocean (EEIO). The MRM derived BLT estimates are compared to gridded Argo and Hybrid Coordinate Ocean Model (HYCOM) BLTs. It is shown that different mechanisms are important for sustaining the BLT variability in each of the selected regions. Sensitivity tests show that SSS is the primary driver of the BLT within the MRM. Results suggest that salinity easurements obtained from Aquarius and SMOS can be useful for tracking and predicting the BLT in the Indian Ocean. Largest MRM errors occur along coastlines and near islands where land contamination skews the satellite SSS retrievals. The BLT evolution during 2012, as well as the advantages and disadvantages of the current model are discussed. BLT estimations using HYCOM simulations display large errors that are related to model layer structure and the selected BLT methodology.

**15. SUBJECT TERMS**
Indian Ocean; barrier layer thickness; Aquarius; SMOS; salinity; HYCOM

| 16. SECURITY CLASSIFICATION OF: a. REPORT | b. ABSTRACT | c. THIS PAGE | 17. LIMITATION OF ABSTRACT | 18. NUMBER OF PAGES | 19a. NAME OF RESPONSIBLE PERSON |
|---|---|---|---|---|---|
| Unclassified | Unclassified | Unclassified | UU | 14 | Jay F. Shriver |
| | | | | | 19b. TELEPHONE NUMBER *(Include area code)* (228) 688-4625 |

Reset

14-1231-2628

PUBLIC[illegible]NTATION RELEASE REQUEST    Pubkey: 927[illegible]    INS [illegible]

Ref: (a) NRL Instruction 5[illegible]0.2
(b) NRL Instruction 5[illegible]10.40D

Encl: (1) Two copies of subject paper (or abstract)

( ) Abstract only, published
( ) Book
( ) Conference Proceedings (refereed)
( ) Invited speaker
( X ) Journal article (refereed)
( ) Oral Presentation, published
( ) Other, explain

( ) Abstract only, not published
( ) Book chapter
( ) Conference Proceedings (not refereed)
( ) Multimedia report
( ) Journal article (not refereed)
( ) Oral Presentation, not published

STRN NRL/JA/7320-14-2210
Route Sheet No. 7320/
Job Order No. 73-8677-03-5
Classification X U C
Sponsor ONR 6.2 BL
approval obtained ___ yes X no

Title of Paper or Presentation
Estimation of the Barrier Layer Thickness in the Indian Ocean Using Aquarius Salinity

Author(s) Name(s) (First,MI,Last), Code, Affiliation if not NRL

Clifford S. Felton Univ. of South Carolina Bulusu Subrahmanyam Univ. of South Carolina V.S.N. Murty CSIR/NIO - India Jay Shriver 7323

It is intended to offer this paper to the ______________________
(Name of Conference)

______________________
(Date, Place and Classification of Conference)

and/or for publication in Journal of Geophysical Research, Unclassified
(Name and Classification of Publication) (Name of Publisher)

After presentation or publication, pertinent publication/presentation data will be entered in the publications data base, in accordance with reference (a).
It is the opinion of the author that the subject paper (is ____ ) (is not X ) classified, in accordance with reference (b).
This paper does not violate any disclosure of trade secrets or suggestions of outside individuals or concerns which have been communicated to the Laboratory in confidence. This paper (does ____ ) (does not X ) contain any militarily critical technology.
This subject paper (has ____ ) (has never X ) been incorporated in an official NRL Report.

Jay Shriver, 7323 [signature]
Name and Code (Principal Author) (Signature)

| CODE | SIGNATURE | DATE | COMMENTS |
|---|---|---|---|
| Author(s) Shriver | [signature] | 26 Jun 14 | Need by 14 July 14 |
| | | | Publicly accessible sources used for this publication |
| | | | This is a Final Security Review. Any changes made in the document, after approved by Code 1231, nullify the Security Review. |
| Section Head Hogan | [signature] | 17 July | |
| Branch Head Gregg A. Jacobs, 7320 | [signature] | 8/4/14 | |
| Division Head Ruth H. Preller, 7300 | [signature] | 8/4/14 | 1. Release of this paper is approved. 2. To the best knowledge of this Division, the subject matter of this paper (has ____ ) (has never X ) been classified. |
| Security, Code 1231 | Sue Fan | 8/4/14 | 1. Paper or abstract was released. 2. A copy is filed in this office. |
| Office of Counsel, Code 1008.3 | Kathy Chapman | 8/11/14 | |
| ADOR/Director NCST E. R. Franchi, 7000 | | | |
| Public Affairs (Unclassified/Unlimited Only), Code 7030.4 | Shannon Menzi | 8-8-14 | |
| Division, Code | | | |
| Author, Code | | | |

NDW-NRL 5511/6 (Rev. 12-98) (e) THIS FORM CANCELS AND SUPERSEDES ALL PREVIOUS VERSIONS

AGU PUBLICATIONS

Journal of Geophysical Research: Oceans

RESEARCH ARTICLE

10.1002/2013JC009759

**Special Section:**
Early scientific results from the salinity measuring satellites Aquarius/SAC-D and SMOS

**Key Points:**

- First study estimating barrier layer using Aquarius and SMOS
- Development of regression model for BLT using satellite data
- Comparison of satellite-derived BLT with HYCOM and Argo

**Correspondence to:**
B. Subrahmanyam,
sbulusu@geol.sc.edu

**Citation:**
Felton, C. S., B. Subrahmanyam, V. S. N. Murty, and J. F. Shriver (2014), Estimation of the barrier layer thickness in the Indian Ocean using Aquarius Salinity, *J. Geophys. Res. Oceans*, *119*, 4200–4213, doi:10.1002/2013JC009759.

Received 20 DEC 2013
Accepted 18 JUN 2014
Accepted article online 23 JUN 2014
Published online 8 JUL 2014

# Estimation of the barrier layer thickness in the Indian Ocean using Aquarius Salinity

**Clifford S. Felton[1], Bulusu Subrahmanyam[1,2], V. S. N. Murty[3], and Jay F. Shriver[4]**

[1]Marine Science Program, University of South Carolina, Columbia, South Carolina, USA, [2]Department of Earth and Ocean Sciences, University of South Carolina, Columbia, South Carolina, USA, [3]Council of Scientific and Industrial Research, National Institute of Oceanography Regional Center, Visakhapatnam, Andhra Pradesh, India, [4]Oceanography Division, Naval Research Laboratory, Stennis Space Center, Mississippi, USA

**Abstract** Monthly barrier layer thickness (BLT) estimates are derived from satellite measurements using a multilinear regression model (MRM) within the Indian Ocean. Sea surface salinity (SSS) from the recently launched Soil Moisture and Ocean Salinity (SMOS) and Aquarius SAC-D salinity missions are utilized to estimate the BLT. The MRM relates BLT to sea surface salinity (SSS), sea surface temperature (SST), and sea surface height anomalies (SSHA). Three regions where the BLT variability is most rigorous are selected to evaluate the performance of the MRM for 2012; the Southeast Arabian Sea (SEAS), Bay of Bengal (BoB), and Eastern Equatorial Indian Ocean (EEIO). The MRM derived BLT estimates are compared to gridded Argo and Hybrid Coordinate Ocean Model (HYCOM) BLTs. It is shown that different mechanisms are important for sustaining the BLT variability in each of the selected regions. Sensitivity tests show that SSS is the primary driver of the BLT within the MRM. Results suggest that salinity measurements obtained from Aquarius and SMOS can be useful for tracking and predicting the BLT in the Indian Ocean. Largest MRM errors occur along coastlines and near islands where land contamination skews the satellite SSS retrievals. The BLT evolution during 2012, as well as the advantages and disadvantages of the current model are discussed. BLT estimations using HYCOM simulations display large errors that are related to model layer structure and the selected BLT methodology.

## 1. Introduction

Salinity stratification and subsequent barrier layer (BL) formation play an important role in regulating surface heat exchanges. Sharp vertical salinity gradients increase the stability of the water column and inhibit thermocline mixing. This limits heat exchange that subsequently warms the upper ocean [*Monetégut et al.*, 2007; *Sengupta et al.*, 2008; *Girishkumar et al.*, 2013]. When the ocean is stratified by salinity, there is a difference between isothermal layer depth (ILD) and mixed layer depth (MLD). The ILD is typically determined by a temperature criterion while the MLD is obtained using the density criterion. The barrier layer thickness (BLT) is then defined as the difference between the ILD and MLD.

*Sprintall and Tomczak* [1992] were the first to study the BL on a global scale and determined that BL formation in the Indian Ocean is driven by the monsoon cycle. Reversing winds, currents, and freshwater fluxes (evaporation (E), precipitation (P), and river runoff (R)) each play a role in the regulating BL development within the Indian Ocean subbasins [*Masson et al.*, 2002; *Qu and Meyers*, 2005; *Durand et al.*, 2007; *Thadathil et al.*, 2007, 2008]. Equatorial waves also impact the formation of the BL due to their interaction with thermocline depth [*Girishkumar et al.*, 2011]. The formation and thickness of the BL has been shown to impact numerous features in the Indian Ocean including the summer monsoon, development of the Indian Ocean Dipole (IOD), and tropical cyclone upwelling in the Indian Ocean [*Masson et al.*, 2005; *Sengupta et al.*, 2008; *Qiu et al.*, 2012; *Balaguru et al.*, 2012; *Guo et al.*, 2013]. As such, tracking the development and movement of the BL is of great interest in this dynamic region.

The launch of National Aeronautics and Space Administration's (NASA) Aquarius Salinity/SAC-D and European Space Agencies (ESA) Soil Moisture Ocean Salinity (SMOS) missions has allowed for global SSS measurements to be made on spatial and temporal scales that were previously logistically impossible. Both satellites have already been able to reveal the SSS structure of many phenomena including tropical instability waves [*Lee et al.*, 2012], a haline hurricane wake from the Amazon River plume [*Grodsky et al.*, 2012],

  

surface freshening events in the Pacific [*Boutin et al*., 2013], the seasonality of salt flux in the Indian Ocean [*Nyadjro et al*., 2013], and the Madden-Julian Oscillation [*Grunsiech et al*., 2013]. With satellites now providing global coverage of SSS, we investigate the feasibility of using SSS with other satellite-derived variables as a proxy for the BLT in the Indian Ocean.

Argo buoys have drastically increased the number of temperature and salinity measurements in ocean basins. In 2005, buoy coverage in the Indian Ocean began meeting Argo program sampling density requirements and float data have been used in many oceanographic studies within the region [e.g., *Nyadjro et al*., 2013]. Since remotely sensed SSS is restricted to the upper few centimeters at the ocean surface, Argo data serve as a reliable reference source to verify satellite SSS and calibrate ocean models.

BLT comparisons between gridded Argo float profiles and estimates using a multilinear regression model (MRM) for three regions in the Indian Ocean are performed. The advantages and disadvantages of the technique are described as well. Simulations from the HYbrid Coordinate Ocean Model (HYCOM) are also used to further evaluate the performance of the MRM in each of the selected regions. The organization of the paper is as follows. Data sources and methodology are presented in section 2 followed by the results in section 3. Section 4 summarizes the results and discusses the implications for using Aquarius and SMOS SSS measurements to understand and track the BL in the Indian Ocean.

## 2. Data and Methodology

### 2.1. Data Sources

Monthly Aquarius SSS version 2.0 Level 3 data from September 2011 to July 2013 are obtained from NASA's Jet Propulsion Laboratory (JPL). In order to produce the Level 3 gridded maps, the converted Aquarius sensor measurements (raw signal to SSS) are binned onto a 1° global grid. Mapped SSS products are computed as averages across all three radiometers as well as individual instrument files (daily to weekly to monthly). Monthly composite, 1° resolution Level 3 SMOS SSS data were obtained from the Ocean Salinity Expertise Center (CECOS) of CNES (Centre National d'Etudes Spatiales)-Ifremer Centre Aval de Traitement des Données SMOS (CATDS), located in Plouzane, France. Both satellites' onboard passive microwave radiometers estimate salinity from sea surface brightness temperature using the L-band (1400–1427 MHz) frequency. Since some gaps are present in the monthly gridded values, an inverse weighted function is used to fill missing open ocean values within 1° (eight surrounding points).

Monthly gridded Argo temperature and salinity profiles from January 2005 to December 2012 are obtained from the Asia Pacific Data-Research Center (APDRC). The data center produces monthly gridded 1° horizontal resolution files from individual float measurements by using a variational interpolation algorithm to minimize the misfit between the interpolated fields and the individual float profiles. Vertical resolution follows World Ocean Atlas (WOA) standard depth levels. MLD and ILD are determined from the gridded data using the criteria by *Sprintall and Tomczak* [1992]. The ILD is defined at the depth where the temperature at depth ($T_z$) reaches $\pm 0.5°$C from the surface value ($T_0$); in this way the presence of thermal inversions (up to $+0.5°$C) are considered. MLD is defined using a variable density criterion as follows:

$$\Delta\sigma=\sigma_t(T_0+\Delta T, S_0, P_0)-\sigma_t(T_0, S_0, P_0) \tag{1}$$

where $\Delta\sigma$ is the difference in density from the surface to the base of the MLD. The first term on the right is the density equal to a change in $\Delta T$ ($\pm 0.5°$C, to account for the presence of thermal inversions) from the surface temperature ($T_0$) while keeping salinity constant, and the second term on the right is the surface $\sigma_t$ value (kg m$^{-3}$). The MLD is then found by searching each profile to find where $\sigma_t$ is equal to surface $\sigma_t + \Delta\sigma$. If the density value falls between two Argo levels, linear interpolation is used to estimate the exact depth (m). The BLT is then defined as the difference between the ILD and MLD (ILD − MLD = BLT). RAMA mooring BLT was examined to compare with Argo BLT for the BoB and EEIO, but incomplete RAMA data over the study period prevented further analysis.

HYCOM simulations for year 2012 were obtained from the real-time data assimilative 1/12° global HYCOM nowcast/forecast system. HYCOM is a next-generation system capable of nowcasting and forecasting the oceanic "weather." Some components include the three-dimensional ocean temperature, salinity and

current structure, the surface mixed layer, and the location of mesoscale features such as eddies, meandering currents, and fronts. HYCOM is isopycnal in the open, stratified ocean, but uses the layered continuity equation to make a dynamically smooth transition to a terrain-following coordinates in shallow coastal regions, and to z-level coordinates in the mixed layer and/or unstratified seas [*Bleck*, 2002]. The system used three hourly forcing from the Navy Operational Global Atmospheric Prediction System. Data assimilation was performed using the Navy Coupled Ocean Data Assimilation (NCODA) [*Cummings*, 2005] system with a model forecast as the first guess. NCODA assimilates available satellite altimeter observations (along track obtained via the NAVOCEANO Altimeter Data Fusion Center), satellite and in situ sea surface temperature (SST), as well as available in situ vertical temperature and salinity profiles from XBTs, Argo floats, and moored buoys. For additional details on the HYCOM nowcast/forecast system, the reader is referred to *Metzger et al*. [2009]. MLD, ILD, and BLT were determined from HYCOM simulations using the same methodology as used for Argo.

Monthly Archiving, Validation, and Interpretation of Satellite Oceanographic (AVISO) sea surface height anomalies (SSHAs) from January 2005 to December 2012 at 1/3° resolution are used as a proxy for thermocline depth in the regression formula. National Oceanic and Atmospheric Administration (NOAA) optimally interpolated monthly sea surface temperature (NOAA OI SST v2) data from January 2005 to December 2012 are also used. The SST monthly fields are derived by a linear interpolation of the weekly optimum interpolation (OI) version 2 fields to daily fields then averaging the daily values over a month with a 1° horizontal resolution [*Reynolds et al*., 2002].

### 2.2. Methodology

Since satellite measurements are restricted to measuring the surface microlayer (top cm), a multilinear regression model is used to relate the remotely sensed products to the BLT. First, all products are linearly interpolated onto a 1° × 1° common grid. The three study regions have the longitude and latitude bounds as follows: SEAS (64.5°E–76.5°E, 4.5°N–13.5°N), BoB (79.5°E–95.5°E, 7.5°N–23.5°N), and EEIO (79.5°E–100.5°E, 5.5°S–5.5°N).

The multilinear regression model (MRM) for estimating the barrier layer thickness is as follows:

$$\mathrm{BLT}=b_0+\alpha_1\mathrm{SSS}+\alpha_2\mathrm{SST}+\alpha_3\mathrm{SSHA} \tag{2}$$

where $b_0$ is the constraint term and $\alpha_{1,2,3}$ are the respective coefficient weights. The constraint term ($b_0$) and each of the coefficients ($\alpha_i$) are computed from the 2005 to 2011 Argo profile derived BLT and SSS, OI SST, and AVISO SSHA values for each month at each grid point. This assumes that the BLT, SSS, and SST are all related to upper ocean stratification and are included as proxies for the MLD. SSHAs from AVISO are used as a proxy for thermocline depth (or ILD) as earlier studies have illustrated the connection between the two parameters [*Shenoi et al*., 2004; *Girishkumar et al*., 2013; *McPhaden and Nagura*, 2013]. Three proxy reconstructions of BLT (ArgoE BLT, Aquarius BLT, SMOS BLT) are then created using monthly Argo and remotely sensed SSS products (Aquarius and SMOS) with OI SST and AVISO SSHAs held constant in each of the BLT models. ArgoE is included to verify the accuracy of the model. If the MRM is perfect, ArgoE BLT should match Argo profile derived BLT precisely. Aquarius BLT and SMOS BLT are shown to demonstrate the ability of the model to reproduce the BLT structure while utilizing SSS from satellite sources. A pictorial diagram of the methodology has been included (Figure 1).

The correlations computed for the thickness (MLD, ILD, and BLT) versus surface variable (SSS, SSHA, and SST) correlations are from each boxed region for the given month over the 2005–2011 time frame. Any missing data are removed before computing the correlations. This resulted in large number of data points (SEAS 130, BoB 289, EEIO 264 for each month then integrated over the 7 year time period) that are used to compute the correlations and significance of those correlations.

## 3. Results

### 3.1. Validation of SSS Data Sources

Before utilizing the MRM, each salinity data source is briefly validated. The distribution of salinity in the Indian Ocean is unique when compared to the other basins with higher salinity in the western contrasted

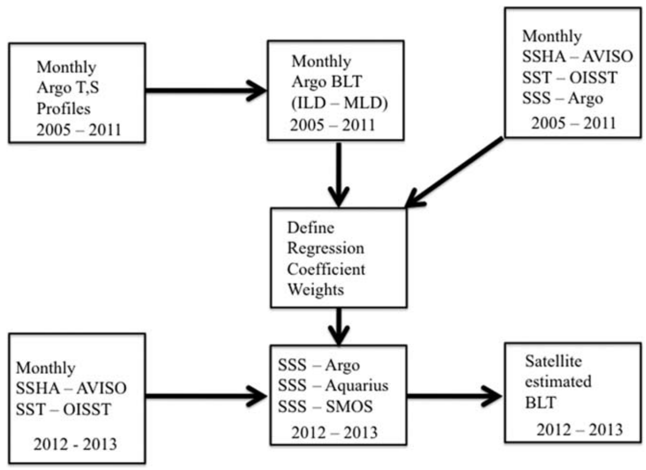


**Figure 1.** Methodology for MRM estimated BLT.

by lower salinity in the eastern regions of the basin (Figure 2). In the Arabian Sea, evaporation (E) greatly exceeds precipitation (P) resulting in high salinity (>36 PSU). Strong seasonal monsoon winds and the large air-sea moisture gradient result in high evaporation rates and the observed higher salinity. In the eastern side of the basin, freshwater inputs into the Bay of Bengal, from river runoff and precipitation, drive seasonally very low salinities (<32 PSU) [*Sengupta et al*., 2006]. Seasonal reversing monsoonal winds also cause waters to exchange between the AS and BoB [*Rao and Sivakumar*, 2003; *Thadathil et al*., 2007; *Vinayachandran et al*., 2013]. The equatorward flowing East India Costal Current (EICC) carries low saline water from the BoB toward the westward flowing North Equatorial Current (NEC) into the Arabian Sea during the winter monsoon season (January–April) (Figure 3a). Conversely during the southwest monsoon season (June–September), the strong eastward flowing South Monsoon Current transports saltier water from the AS into the BoB (Figure 3b) [*Murty et al*., 1992]. A signature of this can be seen north of the equator from 60°E to 95°E in Figure 2 (~35 PSU). Consistent differences exist between Argo and the other SSS sources, especially within the SEAS region (Table 1). In the EEIO, SSS holds nearly constant throughout the year (Figure 3c) except during October and November when the southward shifting ITCZ brings enhanced rainfall over the region causing SSS to slightly drop.

In addition to the yearly mean, Aquarius is able to capture the seasonal cycle well in each of the three study regions (Figures 3a, 3c, and 3e). However, an intercomparison of the four SSS data sets indicates seasonally large SSS deviations in the SEAS and BoB (Figures 3b and 3d). For the SEAS (Figures 3a and 3b), Argo SSS and Aquarius SSS RMSE is lowest during the premonsoon time frame (February–May) and increases from July to December. HYCOM SSS varies similarly. Aquarius SSS is lower than gridded Argo SSS likely due to

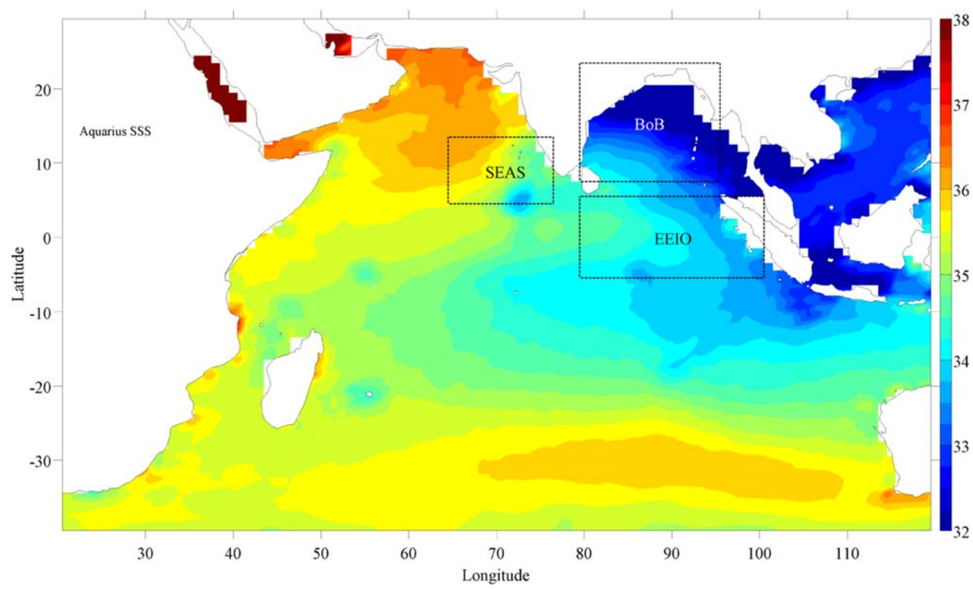


**Figure 2.** Level 3 Aquarius SSS (PSU) for the period from September 2011 to July 2013. Boxes indicate the regions where SSS is validated and BLT estimations are compared. Shading interval is every 0.25 PSU.

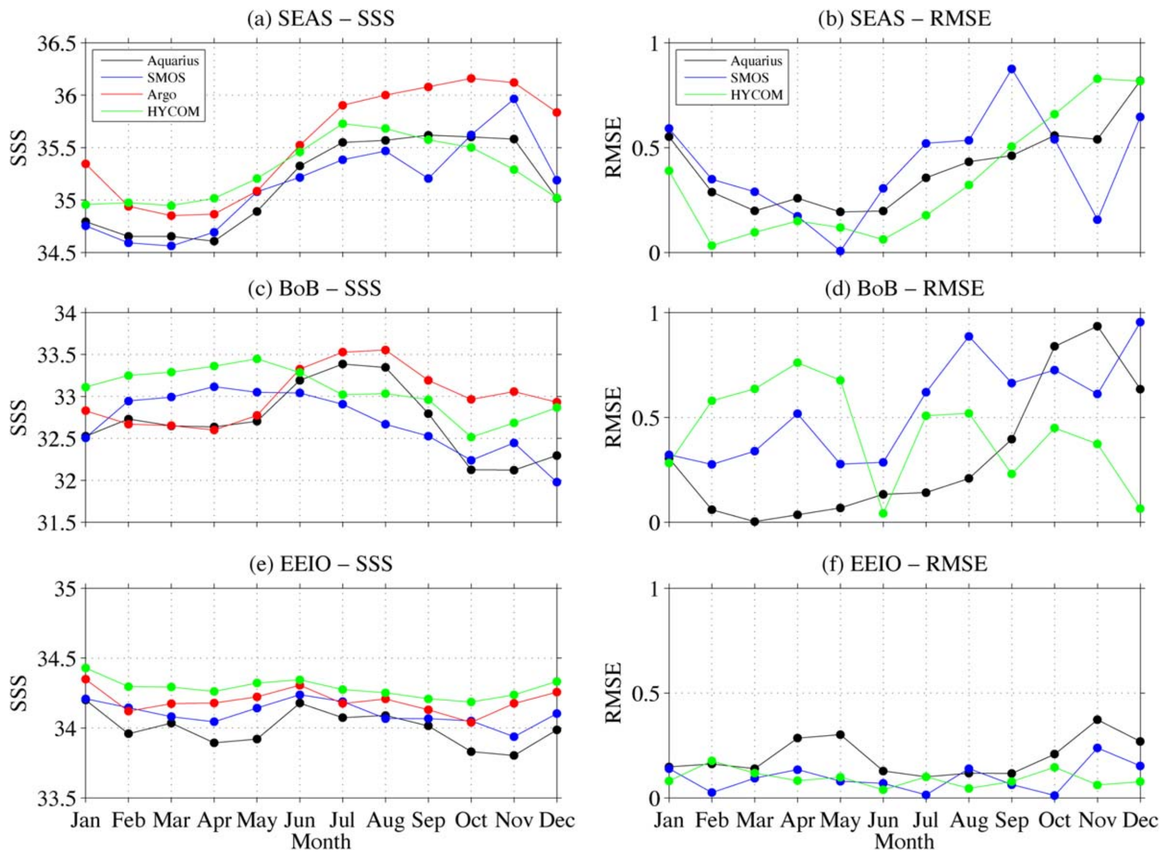


**Figure 3.** Monthly sea surface salinity (SSS) and RMSE (relative to Argo SSS) from January 2012 to December 2012 for the boxes in the (a and b) SEAS, (c and d) BoB, and (e and f) EEIO.

land contamination, precipitation associated with the onset of Indian Summer Monsoon, and the arrival of low saline water from the BoB. This holds true for SMOS as well. For the BoB, SSS deviations are large between the gridded Argo and Aquarius SSS from July to December also (up to ~1 PSU). SMOS SSS exhibits a similar seasonal RMSE pattern, with larger error variations than Aquarius. The increase in RMSE matches well with the seasonal river discharge cycle in the BoB indicating that freshwater influx from the rivers surrounding the BoB are likely producing the errors pattern. EEIO SSS (Figures 3e and 3f) is stable throughout the year among the three data sets, with low monthly RMSE values (<0.4 PSU).

An understanding the spatiotemporal differences between Argo gridded SSS and remotely sensed SSS is also important for evaluating MRM results over the seasonal cycle. Minimal and maximum SSS differences between the products and the corresponding months can be utilized to reveal the source of the SSS errors as well. Maximal differences (>±1 PSU) between the Argo gridded and Aquarius SSS occur in the SEAS and surrounding the BoB (Figure 4a). The differences in the northern BoB are high in August, when river discharge peaks, then move along the east coast of India and into the SEAS region by December (Figure 4c). This indicates that river discharge plays an important role in SSS differences likely due to upper ocean stratification. Large minimum differences in the vicinity of the Maldives between Argo and Aquarius SSS (Figure 4b) confirm that land contamination is occurring year round with minimum differences of at least 1 PSU year round. The southwestern Sumatran

**Table 1.** Sea Surface Salinity (SSS) and RMSE (Relative to Argo SSS)[a]

| | SEAS | | BoB | | EEIO | |
|---|---|---|---|---|---|---|
| Source | SSS | RMSE | SSS | RMSE | SSS | RMSE |
| Argo | 35.6 | | 33.0 | | 34.2 | |
| Aquarius | 35.2 | 0.4 | 32.7 | 0.3 | 34.0 | 0.2 |
| SMOS | 35.1 | 0.4 | 32.7 | 0.3 | 34.1 | 0.1 |
| HYCOM | 35.2 | 0.3 | 33.0 | 0.0 | 34.3 | 0.1 |

[a]SSS is averaged within each selected region from January to December 2012 (PSU).

  

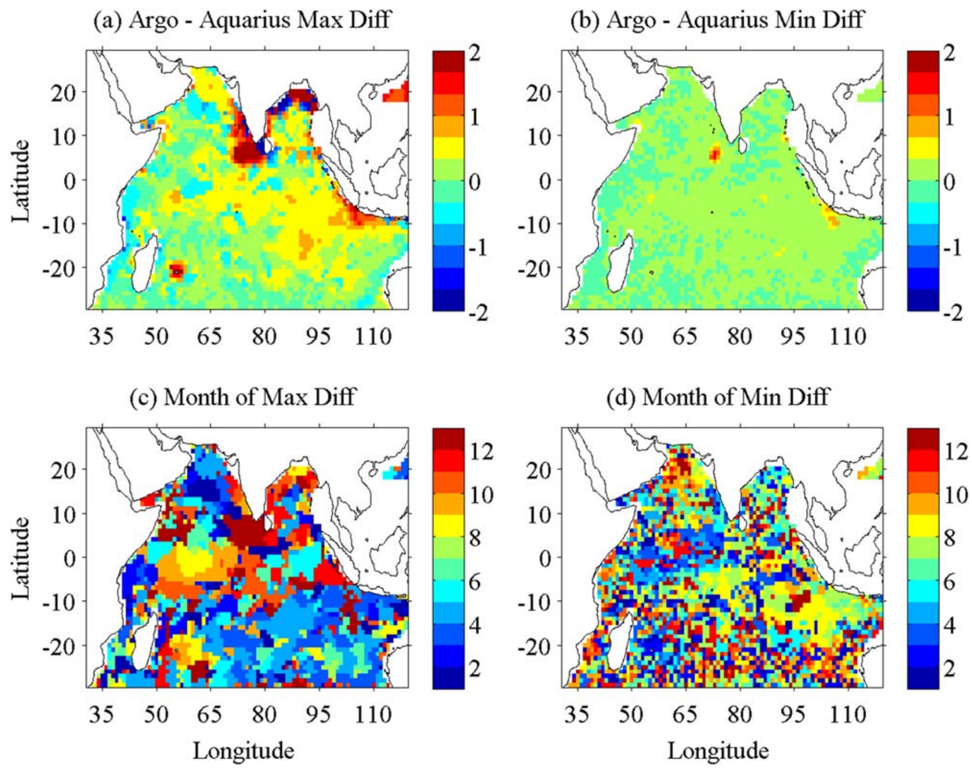


**Figure 4.** (a) Maximum and (b) minimum Argo minus Aquarius SSS differences (diff) over the January–December 2012 time frame. The occurrence (month) of the each grid point difference value, (c) maximum and (d) minimum, is shown below.

coastline is also a region with large SSS deviations (~1 PSU), peaking during November (Figures 4c and 4d) when seasonal precipitation is highest. SSS also varies by at least 0.5 PSU near the Sunda Strait, which may be due to land contamination and/or a consistent low saline water flux through the strait. A full salinity budget would need to be computed to determine the exact source(s) of the differences and will be investigated in a future study. Patterns are similar for SMOS SSS (not shown). Maximal differences are present over the entire North Indian Ocean due to land contamination, with SSS differences following a similar spatio-temporal evolution as Aquarius in the BoB and SEAS.

### 3.2. Description of the BLT Seasonal Cycle

Distinctly different processes drive the BLT seasonal cycle within each of the three study areas. For the SEAS region, the BLT is driven by the seasonal influx of low saline waters from the BoB [*Durand et al*., 2007]. During the winter months (January–March) low saline waters are advected around Sri Lanka shoaling the MLD, while downwelling Rossby and Kelvin waves deepen the ILD resulting in a thick BL (Figure 5a). Rossby and Kelvin waves do not impact the MLD due to the saline stratified surface layer that inhibits mixing [*Thadathil et al*., 2008]. The BL begins to erode with the onset of the summer monsoon when high salinity waters arrive via the equatorward flowing West India Coastal Current (WICC), reducing stratification, and the arrival of remotely forced upwelling Rossby wave fronts that shoal the thermocline [*Shenoi et al*., 2004, 2005].

In the BoB, the BL also peaks during the winter (December–March) when the redistribution of low saline waters from precipitation and river runoff throughout the Bay causes strong upper ocean stratification (Figure 5b). The freshwaters cause strong density stratification in the upper ocean that shoals the MLD while Ekman pumping causes the ILD to deepen [*Thadathil et al*., 2007]. Due to the strong stratification in the upper ocean, Ekman pumping does not significantly impact the MLD, but deepen the ILD [*Shetye et al*., 1996; *McCreary et al*., 1996]. During April–November, upper ocean stratification also supports the development of weather disturbances such as tropical cyclones and monsoon depressions [*Murty et al*., 2000].

In the EEIO, the BL peaks from November to January (c), during the boreal winter period. The combined action of vertical and zonal advection off Sumatra, creating a subsurface salinity maximum, and stratification

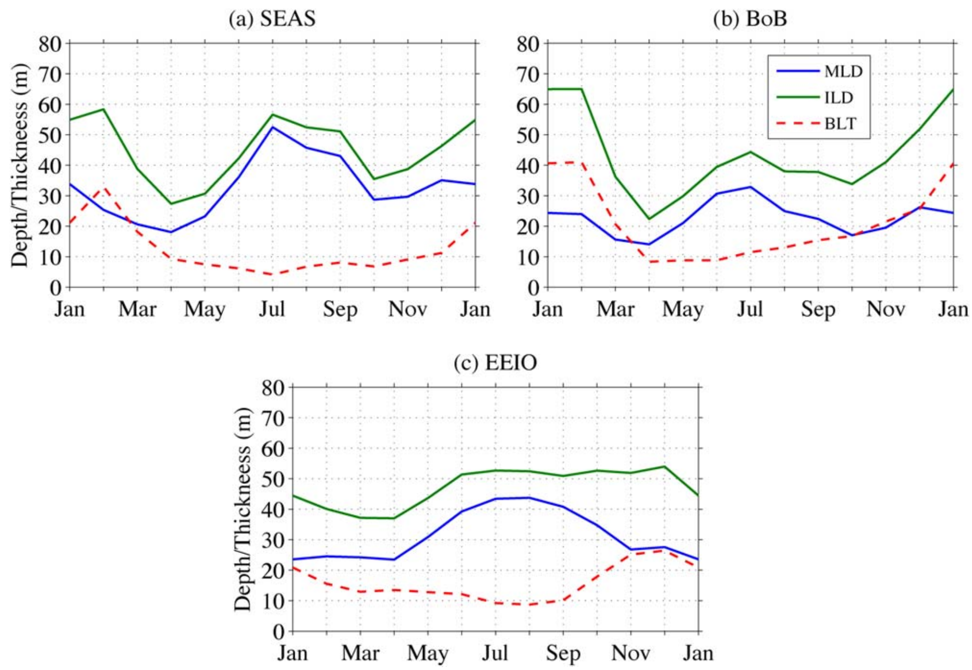


**Figure 5.** The seasonal evolution of the MLD (blue), ILD (green), and BLT (dashed red) for the (a) SEAS, (b) BoB, and (c) EEIO from Argo. January is shown twice to complete the seasonal cycle. BLT in the above figure is computed as the difference between the ILD and MLD averaged from 2005 to 2012 (ILD-MLD).

in the upper ocean due to seasonally high precipitation and runoff, causes the BL to develop [*Masson et al.*, 2002].

### 3.3. Evaluation of Proxy Variables (SSS, SST, and SSHA)

With the validity of the salinity data sources confirmed, the rest of the paper focuses on the results from the regression model. Correlations were run between each of the selected BLT proxy terms (SSS, SST, and SSHA) and the MLD, ILD, and BLT from the Argo data. This is done to ensure that the selected parameters can effectively estimate the BLT in each of the study areas.

In the SEAS region (Table 2), SSS (SST) has high positive (negative) correlations during the southwest and winter monsoon seasons with MLD. The positive MLD correlations with SSS indicate that salinity is important for stratification in this region with higher (lower) salinity creating a deeper (shallower) MLD. The negative relationship between the MLD and SST reveals that higher temperatures result in a shallower MLD due to upper ocean stratification. For much of the year, the ILD and SSHA are positively correlated, implying

**Table 2.** Correlation Coefficients, Southeast Arabian Sea (SEAS)[a]

| SEAS | MLD Versus SSS | MLD Versus SST | ILD Versus SSHA | MLD Versus BLT | ILD Versus BLT | MLD Versus SSHA |
|---|---|---|---|---|---|---|
| Jan. | **0.70** | **−0.29** | **0.45** | **−0.71** | **0.66** | **−0.41** |
| Feb. | **0.38** | **−0.26** | **0.32** | **−0.77** | **0.83** | **−0.35** |
| Mar. | **0.38** | 0.00 | 0.03 | **−0.24** | **0.70** | **−0.20** |
| Apr. | −0.05 | 0.03 | 0.05 | −0.02 | **0.66** | **0.15** |
| May | **−0.22** | **−0.34** | **−0.15** | 0.08 | **0.70** | **−0.11** |
| Jun. | **0.29** | 0.07 | **0.43** | **0.27** | **0.75** | **0.38** |
| Jul. | **0.67** | **−0.13** | **0.55** | **−0.41** | −0.01 | **0.54** |
| Aug. | **0.75** | **−0.46** | **0.55** | **−0.58** | **−0.28** | **0.57** |
| Sep. | **0.54** | **−0.20** | **0.49** | **−0.65** | **−0.18** | **0.45** |
| Oct. | −0.02 | **−0.20** | **−0.28** | **−0.50** | **0.14** | **−0.34** |
| Nov. | **0.34** | **0.18** | **0.37** | **−0.68** | **0.35** | **−0.16** |
| Dec. | **0.64** | **−0.15** | **0.61** | **−0.66** | **0.56** | **−0.15** |

[a]Correlation coefficients of BLT with MLD and ILD and correlation of MLD and ILD with Argo sea surface salinity (SSS), OI sea surface temperature (SST), and AVISO sea surface height anomalies (SSHA) for the Southeast Arabian Sea (SEAS) study region. Data from Argo and are taken from 2005 to 2011. Bold values indicate correlations where the $p$ value $< 0.01$.

**Table 3.** Correlation Coefficients, Bay of Bengal (BoB)[a]

| BoB | MLD Versus SSS | MLD Versus SST | ILD Versus SSHA | MLD Versus BLT | ILD Versus BLT | MLD Versus SSHA |
|---|---|---|---|---|---|---|
| Jan. | **0.63** | **0.37** | **0.13** | **−0.72** | **0.90** | **−0.10** |
| Feb. | **0.66** | **0.48** | 0.02 | **−0.58** | **0.92** | **0.18** |
| Mar. | **0.66** | **0.17** | 0.01 | **0.10** | **0.93** | **0.14** |
| Apr. | **0.45** | **0.11** | 0.07 | **−0.17** | **0.62** | **0.20** |
| May | **0.60** | **−0.37** | **0.15** | 0.08 | **0.58** | **0.20** |
| Jun. | **0.67** | **−0.27** | **0.20** | **−0.51** | **0.54** | 0.04 |
| Jul. | **0.43** | **−0.09** | **0.25** | **−0.63** | **0.21** | **0.09** |
| Aug. | **0.65** | **−0.11** | **0.19** | **−0.61** | 0.06 | −0.02 |
| Sep. | **0.72** | **−0.55** | **0.26** | **−0.62** | **0.18** | 0.04 |
| Oct. | **0.51** | **−0.66** | **0.24** | **−0.48** | **0.61** | 0.02 |
| Nov. | **0.57** | −0.01 | **0.36** | **−0.65** | **0.86** | **−0.14** |
| Dec. | **0.49** | **0.15** | **0.17** | **−0.59** | **0.84** | **−0.22** |

[a]Correlation coefficients of BLT with MLD and ILD and correlation of MLD and ILD with sea surface salinity (SSS), sea surface temperature (SST), and sea surface height anomalies (SSHA) for the Bay of Bengal (BoB) study region. Data from Argo and are taken from 2005 to 2011. Bold values indicate correlations where the $p$ value $< 0.01$.

that a deeper ILD is associated with higher SSHAs, which is physically accurate. Additionally, MLD and SSHA relationships vary with the monsoon seasons. Just prior to and during the summer monsoon (April–September), MLD and SSHA are negatively related while during the winter monsoon (October–March) the relationship becomes positive. BLT is positively correlated with ILD and negatively correlated with MLD. In other words, the relationship indicates that the shallower (deeper) the MLD (ILD), the thicker the BL is, matching expectations. The poor correlations between SSS, SST, and SSHA with MLD and ILD during March–April is likely due to the transitions that occur between the winter and summer monsoon seasons when other factors, such as wind stress and reversing currents, may be driving upper ocean processes that also impact the BLT.

Similar relationships are found between the MLD and SSS in the BoB as well (Table 3). Strong positive relationships indicate that salinity plays an important role in controlling the MLD year round, while the MLD and SST correlations vary with the monsoon season. During the summer monsoon period (May–October), strong winds mix the upper ocean that keep SST cool and the MLD deep. During the winter, winds weaken, mixing decreases, and the MLD becomes positively related to temperature. The correlations between SSHA and the ILD also show relatively higher positive values around the southwest monsoon season. As in the SEAS, the MLD (ILD) holds strong negative (positive) relationships with the BLT throughout much of the year.

In the EEIO, positive correlations are prevalent from boreal summer to winter to spring months (August–April, except in December) between the MLD and SSS (Table 4). Negative correlations are present between the MLD and SST for the same months. This indicates that increased (or deceased) salinity and decreased (or increased) temperatures lead to MLD shoaling. The correlations between the ILD and SSHA also exhibit relatively high positive values for almost all the months (except June). The strong positive correlations are

**Table 4.** Correlation Coefficients, Eastern Equatorial Indian Ocean (EEIO)[a]

| EEIO | MLD Versus SSS | MLD Versus SST | ILD Versus SSHA | MLD Versus BLT | ILD Versus BLT | MLD Versus SSHA |
|---|---|---|---|---|---|---|
| Jan. | **0.52** | **−0.28** | **0.36** | 0.06 | **0.93** | **−0.13** |
| Feb. | **0.43** | **−0.49** | **0.44** | **0.08** | **0.75** | **0.46** |
| Mar. | **0.31** | **−0.42** | **0.53** | **0.22** | **0.81** | **0.49** |
| Apr. | **0.30** | **−0.13** | **0.56** | **−0.09** | **0.84** | **0.46** |
| May | **0.08** | **−0.14** | **0.54** | **−0.13** | **0.74** | **0.40** |
| Jun. | **0.35** | **0.07** | **0.14** | **−0.29** | **0.55** | **0.33** |
| Jul. | −0.05 | **0.19** | **0.25** | **−0.36** | **0.45** | **0.09** |
| Aug. | **0.26** | **0.12** | **0.35** | **−0.53** | **0.31** | **0.18** |
| Sep. | **0.33** | −0.04 | **0.51** | **−0.43** | **0.50** | **0.19** |
| Oct. | **0.37** | **−0.26** | **0.67** | **−0.59** | **0.51** | **0.21** |
| Nov. | **0.30** | **−0.13** | **0.66** | **−0.24** | **0.75** | **0.38** |
| Dec. | 0.05 | 0.02 | **0.67** | **−0.11** | **0.87** | **0.43** |

[a]Correlation coefficients of BLT with MLD and ILD and correlation of MLD and ILD with sea surface salinity (SSS), sea surface temperature (SST), and sea surface height anomalies (SSHA) for the Eastern Equatorial Indian Ocean (EEIO) study region. Data from Argo and are taken from 2005 to 2011. Bold values indicate correlations where the $p$ value $< 0.01$.

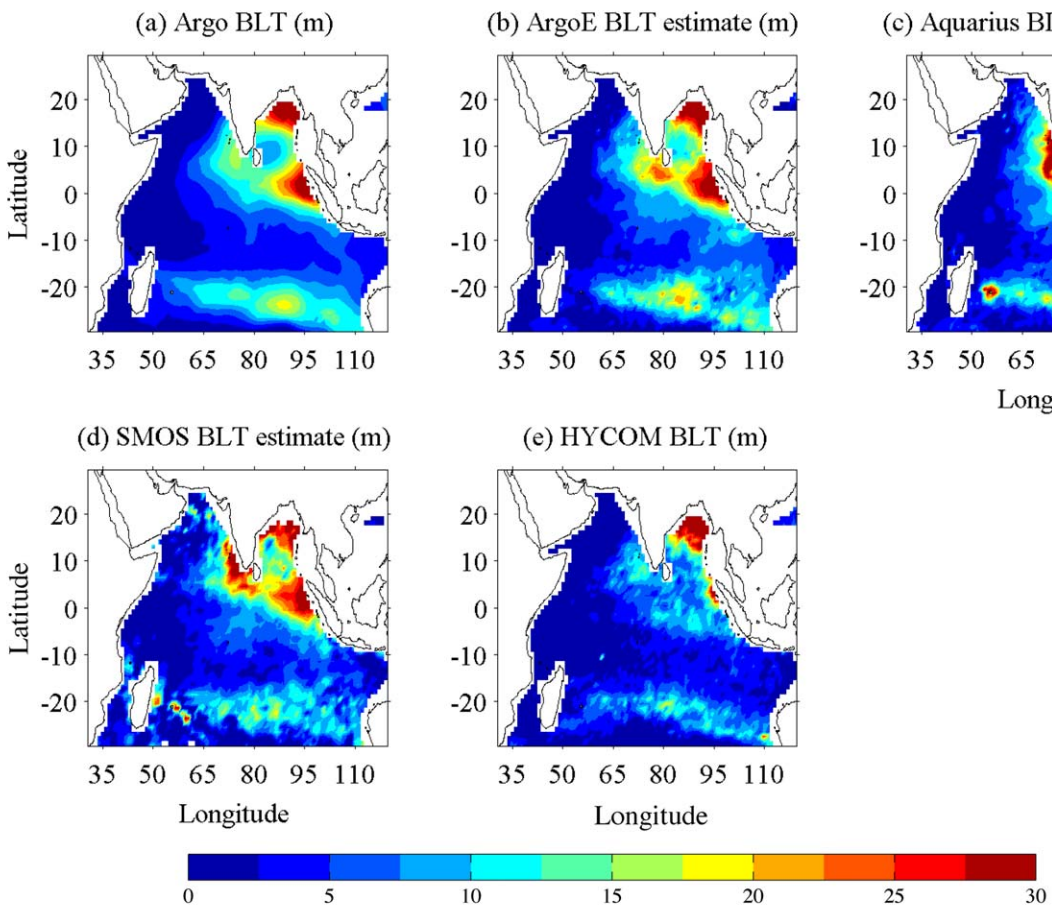


**Figure 6.** Annual mean BLT in the tropical Indian Ocean estimated from (a) Argo BLT (ILD-MLD, and (b) multilinear regression model BLT using Argo SSS (ArgoE), (c) using Aquarius SSS, (d) using SMOS SSS, and (e) using HYCOM. Shading interval is every 2.5 m. SSHA and OISST are kept constant for Figures 6b–6d from equation (2).

due to the presences of equatorial waves in this region that have been shown to relate to SSHA and ILD oscillations [*Hong et al*., 2008]. As in the other two regions, the BLT is positively correlated with the ILD and negatively correlated with the MLD. Due to the negative relationship between the BLT and MLD, this indicates that the shoaling of the MLD, coupled with the deepening of the ILD, leads to thick BL formation.

### 3.4. MRM and HYCOM Results

Yearly averaged spatial patterns agree well between the Argo BLT (MLD-ILD) values (Figure 6a), each of the MRM estimations (Figures 6b–6d), and HYCOM simulations (Figure 6e). Each of the MRMs is able to resolve thick barrier layer formation throughout the Indian Ocean including along the Sumatra coastline, in the Bay of Bengal, and in the SEAS region. Both satellite sources (Aquarius and SMOS) appear to overestimate the BLT within the SEAS. Aquarius results also indicate a thick BL in the vicinity of the Sunda Strait (between Sumatra and Java) that is missing in the rest of the sources due to presence of a low salinity surface plume in the Aquarius data.

In order to investigate any seasonal trends, model BLT estimates for each of the three-boxed regions were averaged for each month. In the SEAS BLT peaks during the boreal winter months due to the influx of low saline water from the BoB (Figure 7a) and arrival of the second downwelling coastally trapped Kelvin wave [*Nienhaus et al*., 2012]. Both Aquarius and SMOS greatly overestimate the BLT during January, February, and September through December (Figure 7b). This BLT error stems from the SSS differences between Argo and remotely sensed SSS products. Both Aquarius and SMOS indicate SSS nearly 0.5 PSU lower than Argo during February. During this time, stratification in the upper ocean is strong and causes large differences between Argo and remotely sensed SSS that result in significant model errors ($\sim$20 m). A similar situation occurs in

  

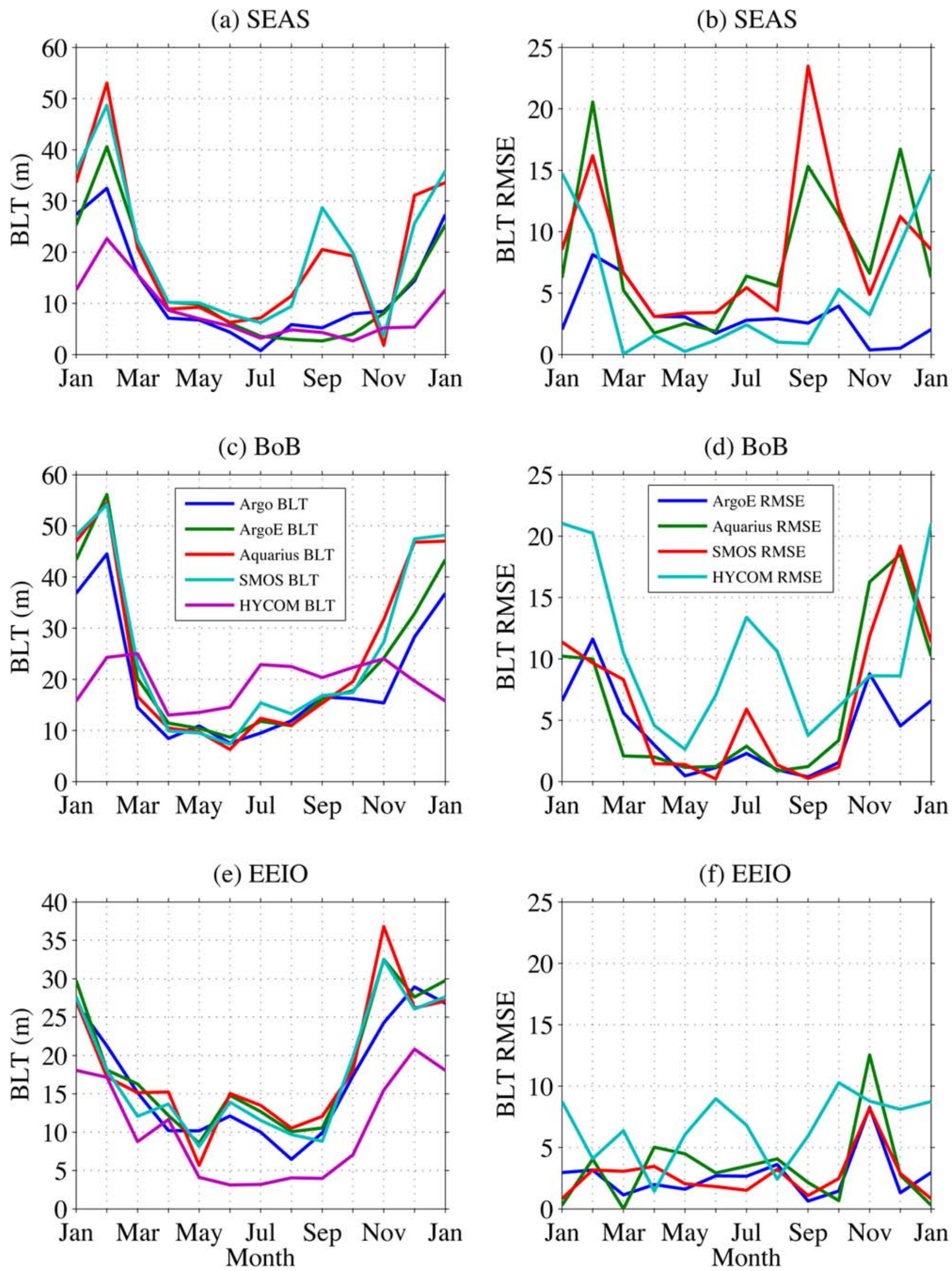


**Figure 7.** (left) Seasonal cycle of box averaged BLT and (right—relative to Argo BLT) RMSE from Argo, MRM estimations, and HYCOM in the (a and b) Southeast Arabian Sea, (c and d) Bay of Bengal, and (e and f) Eastern Equatorial Indian Ocean for 2012. January is shown twice to complete the seasonal cycle.

September when retreat of the SW monsoon creates low salinities at the ocean surface, resulting in lower satellite SSS and large MRM BLT errors. Small islands in the region (such as the Maldives) are also a factor that may be skewing satellite SSS retrievals, as discussed earlier and shown in Figure 4.

Moving to the BoB, model estimations are comparatively better (Figure 7c). Each model captures the seasonal cycle very well with errors largest from November to February (Figure 7d). Salinity errors are largest in November and December, which explain poor model performance during these months. The other peak error months (January–February) indicate that small SSS variations may be responsible for BLT formation. Despite relatively small differences between Argo and satellite SSS, BLT errors are large. It is possible that the inclusion of an Ekman pumping term may improve the model estimations, but due to the lack of a

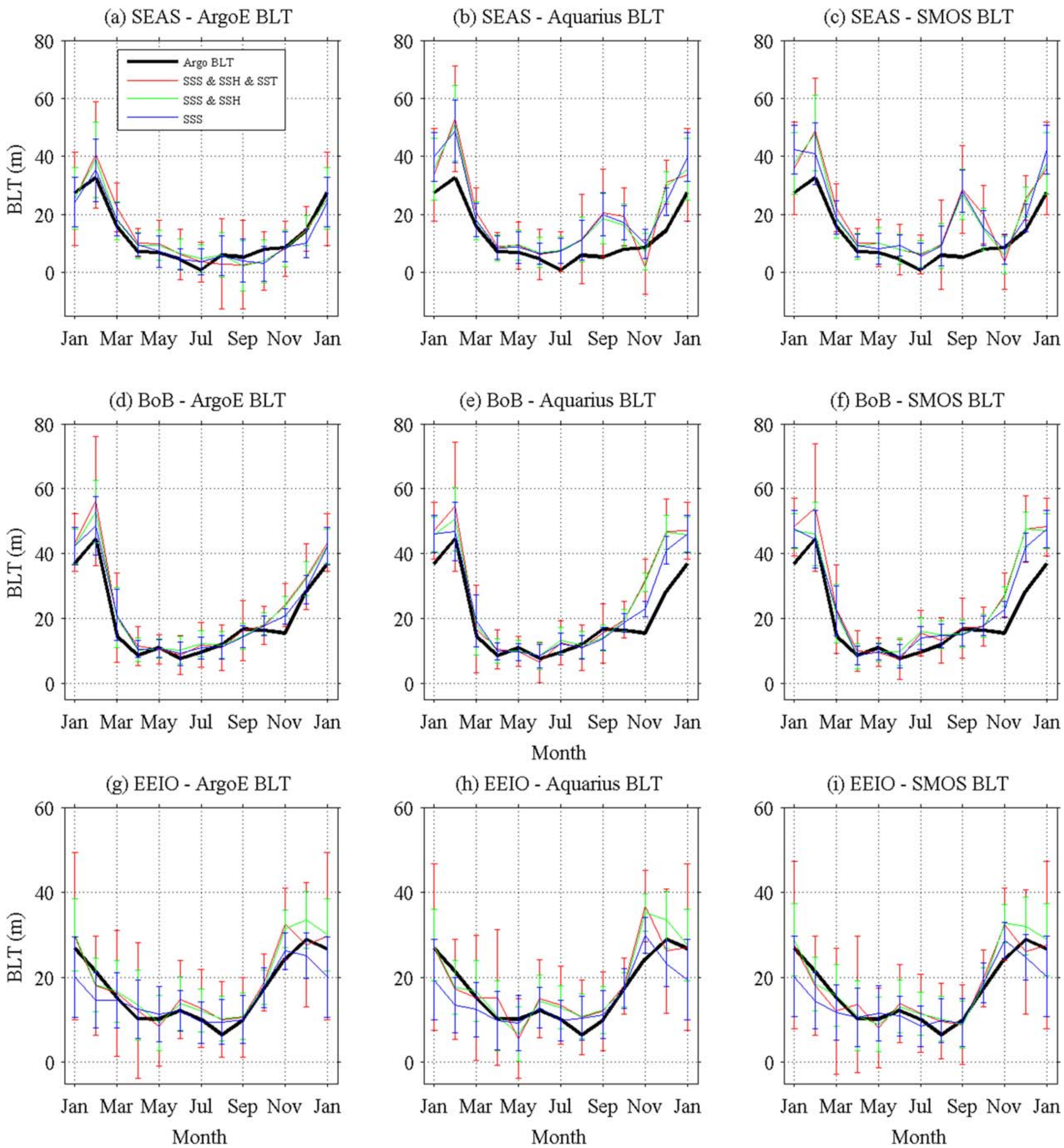


**Figure 8.** Seasonal cycle of BLT in the year 2012 as derived from gridded Argo profiles (black), MRM model with SSS, SSHA, SST (red), MRM model with SSS, SSHA (green), and MRM model with SSS only (blue). Error bars have been included for each MRM BLT estimate based upon the coefficient(s) error(s) (alpha—0.995). January is repeated to complete the seasonal cycle.

continuous satellite record from a single sensor (2005–2013), this term was left out. Future efforts could include wind stress from numerical weather prediction in order to account for this physical process that may improve BLT estimates.

Errors in the EEIO are the smallest among the study regions (Figure 7e). The maximum error occurs in November when nonlinear effects from seasonally high equatorial wave activity may be causing the divergence between MRM and Argo BLT (from ILD-MLD) values (Figure 7f). However, errors are still small in magnitude throughout the year indicating that the MRM is able to accurately determine the presence of a BL within the EEIO.

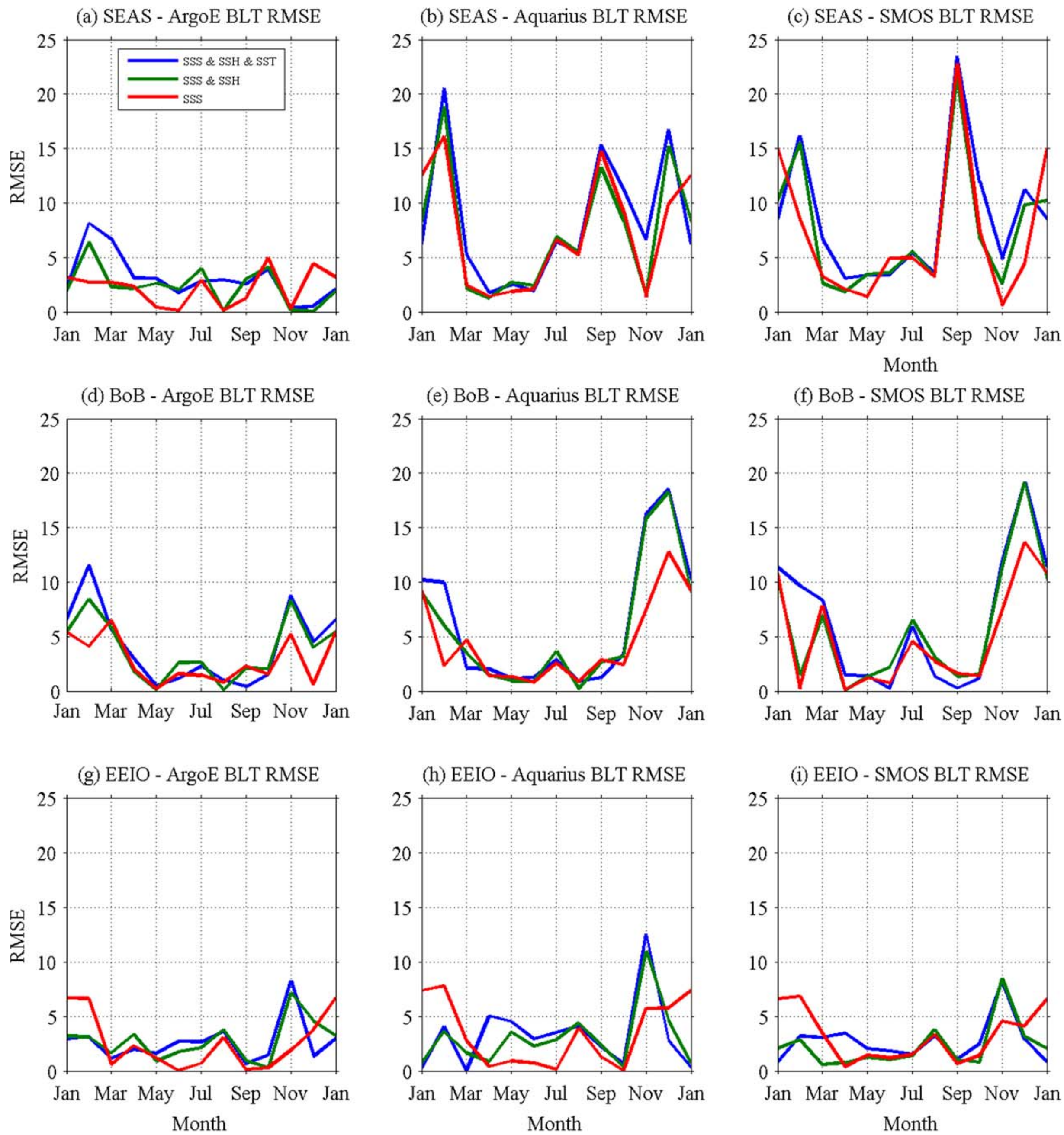


**Figure 9.** Seasonal cycle of RMSE (with respect to Argo gridded profile derived BLT) BLT in the year 2012 for MRM model with SSS, SSHA, SST (red), MRM model with SSS, SSHA (green), and MRM model with SSS only (blue). January is repeated to complete the seasonal cycle.

Sensitivity tests are performed to test the robustness of the variable selections for the MRM model. BLT time series are created with the removal of select variables from equation (2). Two additional models, the partial (SSS and SSH), and SSS only MRMs, are able to reproduce the same seasonal cycle as the full model in each of the regions (Figure 8). When examining the RMSE plots a temporal importance of each variable is noticeable (Figure 9). In each region, the SSS only model performs best on average, with the full (SSS, SSHA, and SST) and partial models (SSS and SSHA) outperforming the SSS only model during select months. This is supported by the error bounds (Figure 8), which indicate that the SSS only model has the least BLT estimation error when accounting for coefficient errors. This demonstrates that SSS, on average, is the main variable driving BLT variations in each of the three study regions. The full and partial models are more accurate than the SSS only model during the months when Rossby and Kelvin waves are climatologically prevalent.

## 4. Discussion and Conclusions

Estimates of the barrier layer thickness in the Indian Ocean are shown utilizing satellite measurements for the first time. A multilinear regression model (MRM) is used to relate satellite-derived SSS, SST, and SSHA to the BLT. This method offers an alternative to Argo floats for determining the presence and thickness of the BL within three regions in the Indian Ocean. The results from the model indicate that satellite SSS measurements can be used in such predictions. The model performs well in each of the three study regions and is able to capture the seasonal cycle well however, significant differences exist within the SEAS. As such, the model serves well as a qualitative indicator of BLT presence as opposed to a measure of the exact BLT magnitude in the SEAS. This is likely due to the complexity of surface and subsurface processes that are not linearly related to the BLT in this region which include the subduction of high saline Arabian Sea water, thermocline response to interacting Rossby wave trains off Sri Lanka, upwelling/downwelling from the Laccadive high, and interactions from the Maldives. MRM sensitivity tests also suggest that SSS is the primary variable responsible for BLT presence.

HYCOM is also shown to have difficulties representing the BLT in the Indian Ocean as a whole. The development of thick isopycnal layers beneath the thinner surface layers in areas of strong density stratification may be the primary source of error. Z-layer spacing in the open ocean in the model is set to at 0, 1, 3, and 6 m depth. Beneath 6 m, depths are based upon isopycnic coordinates that have large spatial variations in the Indian Ocean due to strong density stratification, especially within the BoB. The very thick isopycnal layers (>150 m in the BoB) leads to large ambiguities in the MLD and ILD calculations that then rely more heavily on interpolation in order to convert from the native hybrid coordinate system that HYCOM uses to z levels. The addition of more near-surface model layers or the use of a different MLD/ILD criterion could help overcome this issue however, for this study the definitions are kept constant across data sets (Argo and HYCOM) to ensure an accurate comparison between the products. The reliance on interpolation in the MLD/ILD criteria is likely the largest contributor to poor HYCOM BLT performance relative to Argo.

Based upon the MRM results, assimilating satellite-derived SSS into ocean models with mixing parameterizations schemes (e.g., HYCOM) would likely aid in detecting and tracking the BL in the Indian Ocean. The BLT plays an important role in the evolution and strength of the Indian Ocean Dipole [*Qiu et al*., 2012], the Indian summer monsoon [*Masson et al*., 2005], and tropical cyclones [*Yu and McPhaden*, 2011; *Balaguru et al*., 2012] and utilizing satellite SSS will further scientific understanding of these important processes. Given the success in this preliminary effort, future efforts will be directed toward assimilating satellite SSS into ocean circulation models to better resolve the BLT in the Indian Ocean and to quantify the impact of the BLT on air-sea processes. The continued improvement of satellite retrieved SSS accuracy will also aid in tracking riverine discharge and may also be used to understand freshwater and saltwater budgets in this dynamic region.

**Acknowledgments**
Aquarius version 2.0 data were provided by NASA/JPL PO. DAAC. The HYCOM model simulations were obtained from the Naval Research Laboratory, Stennis Space Center, Mississippi. This work is supported by the NASA Physical Oceanography Award NNX13AM60G awarded to BS. The SMOS Level 3 data were obtained from the Ocean Salinity Expertise Center (CECOS) of the CNES-IFREMER Centre Aval de Traitement des Données SMOS (CATDS), at IFREMER, France. The authors would like to thank both the ESA and SMOS teams for providing Level 3 Ocean Salinity data and support. Monthly gridded Argo temperature and salinity profiles were obtained from the Asia Pacific Data-Research Center (APDRC). One of the authors, VSNM, is thankful to the Director, CSIR-NIO for his keen interest in the joint-collaborative research with BS at the University of South Carolina, Columbia, USA. The authors would also like to thank the editor and two anonymous reviewers whose comments significantly improved the quality of this manuscript. This manuscript has the NIO contribution number 5607.

## References

Balaguru, K., P. Chang, R. Saravanan, L. R. Leung, Z. Xu, M. Li, and J. S. Hsieh (2012), Ocean barrier layers' effect on tropical cyclone intensification, *Proc. Natl. Acad. Sci. U. S. A.*, *109*(36), 14,343–14,347, doi:10.1073/pnas.1201364109.

Bleck, R. (2002), An oceanic general circulation model framed in hybrid isopycnic-Cartesian coordinates, *Ocean Modell.*, *37*, 55–88.

Boutin, J., N. Martin, G. Reverdin, X. Yin, and F. Gaillard (2013), Sea surface freshening inferred from SMOS and ARGO salinity: Impact of rain, *Ocean Sci.*, *9*, 183–192, doi:10.5194/os-9–183-2013.

Cummings, J. A. (2005), Operational multivariate ocean data assimilation, *Q. J. R. Meteorol. Soc.*, *131*, 3583–3604.

Durand, F., D. Shankar, C. de Boyer Montégut, S. S. C. Shenoi, B. Blanke, and G. Madec (2007), Modeling the barrier-layer formation in the southeastern Arabian Sea, *J. Clim.*, *20*, 2109–2120, doi:10.1175/JCLI4112.1.

Girishkumar, M. S., M. Ravichandran, M. J. McPhaden, and R. R. Rao (2011), Intraseasonal variability in barrier layer thickness in the south central Bay of Bengal, *J. Geophys. Res.*, *116*, C03009, doi:10.1029/2010JC006657.

Girishkumar, M. S., M. Ravichandran, and M. J. McPhaden (2013), Temperature inversions and their influence on the mixed layer heat budget during the winters of 2006–2007 and 2007–2008 in the Bay of Bengal, *J. Geophys. Res. Oceans*, *118*, 2426–2437, doi:10.1002/jgrc.20192.

Grodsky, S. A., N. Reul, G. Lagerloef, G. Reverdin, J. A. Carton, B. Chapron, Y. Quilfen, V. N. Kudryavtsev, and H.-Y. Kao (2012), Haline hurricane wake in the Amazon/Orinoco plume: AQUARIUS/SACD and SMOS observations, *Geophys. Res. Lett.*, *39*, L20603, doi:10.1029/2012GL053335.

Grunseich, G., B. Subrahmanyam, and B. Wang (2013), The Madden-Julian oscillation detected in Aquarius salinity observations, *Geophys. Res. Lett.*, *40*, 5461–5466, doi:10.1002/2013GL058173.

Guo, F., Q. Lui, X.-T. Zheng, and S. Sun (2013), The role of barrier layer in Southeastern Arabian Sea during the development of positive Indian Ocean dipole events, *J. Ocean Univ. China*, *12*(2), 245–252, doi:10.1007/s11802-013-2170-4.

Hong, C.-C., T. Li, LinHo, and J.-S. Kug (2008), Asymmetry of the Indian Ocean dipole. Part I: Observational analysis, *J. Clim.*, *21*, 4834–4848, doi:10.1175/2008JCLI2222.1.

Lee, T., G. Lagerloef, M. M. Gierach, H.-Y. Kao, S. Yueh, and K. Dohan (2012), Aquarius reveals salinity structure of tropical instability waves, *Geophys. Res. Lett.*, *39*, L12610, doi:10.1029/2012GL052232.

Masson, S., P. Delecluse, J.-P. Boulanger, and C. Menkes (2002), A model study of the seasonal variability and formation mechanisms of the barrier layer in the eastern equatorial Indian Ocean, *J. Geophys. Res.*, *107*(C12), 8017, doi:10.1029/2001JC000832.

Masson, S., et al. (2005), Impact of barrier layer on winter-spring variability of the southeastern Arabian Sea, *Geophys. Res. Lett.*, *32*, L07703, doi:10.1029/2004GL021980.

McCreary, J. P., W. Han, D. Shankar, and S. R. Shetye (1996), Dynamics of the East India Coastal Current. 2: Numerical solutions, *J. Geophys. Res.*, *101*(C6), 13,993–14,010, doi:10.1029/96JC00560.

McPhaden, M., and M. Nagura (2013), Indian Ocean dipole interpreted in terms of recharge oscillator theory, *Clim. Dyn.*, *42*, 1569–1586, doi:10.1007/s00382-013-1765-1.

Metzger, E. J., H. E. Hurlburt, A. J. Wallcraft, O. M. Smedstad, J. A. Cummings, and E. P. Chassignet (2009), *Predicting "Ocean Weather" Using the HYbrid Coordinate Ocean Model (HYCOM)*, pp. 202–206, Nav. Res. Lab. Rev., Washington, D. C.

Montégut, C. B., J. Vialard, S. S. C. Shenoi, D. Shankar, F. Durand, C. Ethé, and G. Madec (2007), Simulated seasonal and interannual variability of the mixed layer heat budget in the Northern Indian Ocean, *J. Clim.*, *20*, 3249–3268, doi:10.1175/JCLI4148.1.

Murty, V. S. N., Y. V. B. Sarma, D. P. Rao, and C. S. Murthy (1992), Water characteristics, mixing and circulation in the Bay of Bengal during southwest monsoon, *J. Mar. Res.*, *50*, 207–228.

Murty, V. S. N., M. S. S. Sarma, and V. Tilvi (2000), Seasonal cyclogenesis and the role of near surface stratified layer in the Bay of Bengal, *PORSEC Proc.*, *1*, 453–457.

Nienhaus, M. J., B. Subrahmanyam, and V. S. N. Murty (2012), Altimetric observations and model simulations of coastal Kelvin Waves in the Bay of Bengal, *Mar. Geod.*, *35*(1), 190–216. doi:10.1080/01490419.2012.718607,.

Nyadjro, E., B. Subrahmanyam, and B. S. Giese (2013), Variability of salt flux in the Indian Ocean during 1960–2008, *Remote Sens. Environ.*, *134*, 175–193, doi:10.1016/j.rse.2013.03.005.

Qiu, Y., W. Cai, L. Li, and X. Guo (2012), Argo profiles variability of barrier layer in the tropical Indian Ocean and its relationship with the Indian Ocean Dipole, *Geophys. Res. Lett.*, *39*, L08605, doi:10.1029/2012GL051441.

Qu, T., and G. Meyers (2005), Seasonal variation of barrier layer in the southeastern tropical Indian Ocean, *J. Geophys. Res.*, *110*, C11003, doi:10.1029/2004JC002816.

Rao, R. R., and R. Sivakumar (2003), Seasonal variability of sea surface salinity and salt budget of the mixed layer of the north Indian Ocean, *J. Geophys. Res.*, *108*(C1), 3009, doi:10.1029/2001JC000907.

Reynolds, R. W., N. A. Rayner, T. M. Smith, D. C. Stokes, and W. Wang (2002), An improved in situ and satellite SST analysis for climate, *J. Clim.*, *15*, 1609–1625.

Sengupta, D., G. N. Bharath Raj, and S. S. C. Shenoi (2006), Surface freshwater from Bay of Bengal runoff and Indonesian throughflow in the tropical Indian Ocean, *Geophys. Res. Lett.*, *33*, L22609, doi:10.1029/2006GL027573.

Sengupta, D., B. R. Goddalehundi, and D. S. Anitha (2008), Cyclone-induced mixing does not cool SST in the post-monsoon north Bay of Bengal, *Atmos. Sci. Lett.*, *9*, 1–6, doi:10.1002/asl.162.

Shenoi, S. S. C., D. Shankar, and S. R. Shetye (2004), Remote forcing annihilates barrier layer in southeastern Arabian Sea, *Geophys. Res. Lett.*, *31*, L05307, doi:10.1029/2003GL019270.

Shenoi, S. S. C., V. V. Gopalakrishna, and F. Durand (2005), Role of ocean in the genesis and annihilation of the core of the warm pool in the southeastern Arabian Sea, *Mausam*, *56*, 147–160.

Shetye, S. R., A. D. Gouveia, D. Shankar, S. S. C. Shenoi, P. N. Vinayachandran, D. Sundar, G. S. Michael, and G. Nampoothiri (1996), Hydrography and circulation in the western Bay of Bengal during the northeast monsoon, *J. Geophys. Res.*, *101*(C6), 14,011–14,025, doi:10.1029/95JC03307.

Sprintall, J., and M. Tomczak (1992), Evidence of the barrier layer in the surface layer of the tropics, *J. Geophys. Res.*, *97*(C5), 7305–7316, doi:10.1029/92JC00407.

Thadathil, P., P. M. Muraleedharan, R. R. Rao, Y. K. Somayajulu, G. V. Reddy, and C. Revichandran (2007), Observed seasonal variability of barrier layer in the Bay of Bengal, *J. Geophys. Res.*, *112*, C02009, doi:10.1029/2006JC003651.

Thadathil, P., P. Thoppil, R. R. Rao, P. M. Muraleedharan, Y. K. Somayajulu, V. V. Gopalakrishna, R. Murtugudde, G. V. Reddy, and C. Revichandran (2008), Seasonal variability of the observed barrier layer in the Arabian Sea, *J. Phys. Oceanogr.*, *38*, 624–638, doi:10.1175/2007JPO3798.1.

Vinayachandran, P. N., D. Shankar, S. Vernekar, K. K. Sandeep, P. Amol, C. P. Neema, and A. Chatterjee (2013), A summer monsoon pump to keep the Bay of Bengal salty, *Geophys. Res. Lett.*, *40*, 1777–1782, doi:10.1002/grl.50274.

Yu, L., and M. J. McPhaden (2011), Ocean preconditioning of cyclone Nargis in the Bay of Bengal: Interaction between Rossby waves, surface fresh waters, and sea surface temperatures, *J. Phys. Oceanogr.*, *41*, 1741–1755, doi:10.1175/2011JPO4437.1.